Floquet Weyl fermions in three-dimensional stacked graphene systems irradiated by circularly polarized light

Jin-Yu Zou and Bang-Gui Liu*

Beijing National Laboratory for Condensed Matter Physics, Institute of Physics, Chinese Academy of Sciences, Beijing 100190, China

(Received 26 January 2016; revised manuscript received 9 May 2016; published 24 May 2016)

Using Floquet theory, we illustrate that Floquet Weyl fermions can be created in three-dimensional stacked graphene systems irradiated by circularly polarized light. One or two semi-Dirac points can be formed due to overlapping of Floquet subbands. Each pair of Weyl points have a two-component semi-Dirac point parent, instead of a four-component Dirac point parent. Decreasing the light frequency will make the Weyl points move in the momentum space, and the Weyl points can approach to the Dirac points when the frequency becomes very small. The frequency-amplitude phase diagram is worked out. It is shown that there exist Fermi arcs in the surface Brillouin zones in semi-infinitely stacked and finitely multilayered graphene systems irradiated by circularly polarized light. The Floquet Weyl points emerging due to the overlap of Floquet subbands provide a new platform to study Weyl fermions.

DOI: 10.1103/PhysRevB.93.205435

I. INTRODUCTION

As an important fundamental particle, the Weyl fermion has been studied in high-energy physics for a long time, but has not been found in nature yet [1]. Nevertheless, in condensed matter physics, the Weyl fermion can emerge as a quasiparticle in the so called Weyl semimetal (WSM) [2,3]. This phenomenon is analogous to Dirac points in graphene with band crossing and linear dispersion. Recently, the Weyl semimetal, with its novel properties, triggered enormous research activities [2–19], especially the milestone experimental discovery of Weyl fermions [20–22]. Contrasting with the Dirac points in two-dimensional (2D) graphene, Weyl fermions in a 3D semimetal are topologically stable, because the Hamiltonian uses up all three Pauli matrices so that any perturbation can just move the Weyl points unless they meet and annihilate with others with opposite topological numbers [3]. The topological property of WSM protects its surface gapless states which appear in the form of a Fermi arc [5–7]. The Fermi arc connects the projections in the surface Brillouin zone of opposite Weyl points. WSM also exhibits many other interesting phenomena, such as a chiral anomaly [2,10], anomalous Hall effect [7], negative magnetoresistance under parallel electric and magnetic fields, and others [10,23].

In quantum field theory, a massless four-component Dirac fermion can be reduced to two two-component Weyl fermions, which enables one to define a new good quantum number according to their respective chiralities [24]. In condensed matter physics, Weyl fermions can be created in a similar way [4–12,25]. For this purpose, one should find matter with a four-component massless Dirac point band structure, which means that the energy bands should touch each other at the Dirac point with quadruple degeneracy and disperse linearly. The degeneracy of the Weyl points is protected by time-reversal symmetry and inversion symmetry. Breaking any of them will split them and create two Weyl points. In this sense, the Weyl point has a four-component Dirac parent.

Here, however, we will create Weyl fermions with a two-component semi-Dirac parent in a 3D lattice, a stacked graphene system irradiated by circularly polarized light. We use Floquet theory to solve this system, without requiring a high-frequency limit as usual [25]. When the frequency of light is very large compared to the hopping parameters of lattice, Floquet subbands are far from each other. With decreasing frequency, subbands can get closer and closer to touching and overlapping, and then separating and so forth [26–30]. Our investigation shows that with the frequency decreasing, each time the ± 1 Floquet subbands touch, a semi-Dirac point will be created and then split into two Weyl points with opposite chirality, producing two Weyl fermions. A frequency-amplitude phase diagram is completed. It is interesting that there can be such Weyl fermions in the limit of low light amplitude. It is also shown that when a good surface is made, a Fermi arc can be created in the surface Brillouin zone. More detailed results will be presented in the following.

II. MODEL AND FLOQUET THEORY

We define $\vec{\delta}_1$ to point in the x direction and $\vec{a}_1$ the y direction, with the z direction being perpendicular to the layer plane. The three-dimensional lattice model consists of infinite graphene layers, each of which can be considered to be translated from its nearest graphene layer by the vector $\vec{a}_3$ in the x-z plane [31], as demonstrated in Fig. 1. The angle θ is used to parametrize the stacking and $\theta = 90^\circ$ corresponds to the well-known ABC stacking. Our structural model can be considered to be a generalized ABC stacking model with θ being near 90°. We consider only the nearest-neighbor (NN) hopping constants within each layer and between the nearest layers. The light travels in the y direction, with its vector potential being in the x-z plane:

$$\mathbf{A}(t) = A_0(\sin wt, 0, \cos wt). \tag{1}$$

By the Perierls substitution, $\mathbf{k} \to \tilde{\mathbf{k}} = \mathbf{k} + \mathbf{A}(t)$, we can obtain the time-dependent Hamiltonian,

$$H(\mathbf{k},t) = \begin{pmatrix} 0 & h_{12}(\mathbf{k},t) \\ h_{21}(\mathbf{k},t) & 0 \end{pmatrix}, \tag{2}$$

where $h_{12}(\mathbf{k},t)$ is defined as $\gamma \sum_n e^{i[\mathbf{k}+\mathbf{A}(t)]\cdot\delta_n} + \eta e^{i[\mathbf{k}+\mathbf{A}(t)]\cdot\mathbf{d}}$, and $h_{21}(\mathbf{k},t)$ is the complex conjugate of $h_{12}(\mathbf{k},t)$. γ is used to

*bgliu@iphy.ac.cn

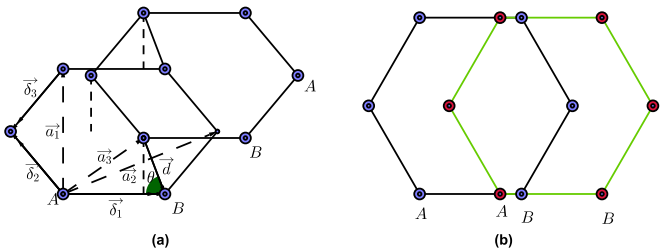

FIG. 1. A schematic of the three-dimensional stacked graphene model which can be built by stacking infinite graphene layers. Panel (a) shows the relation between the two nearest graphenes. The interlayer distance is eqivalent to $d\sin\theta$. The sliding displacement between the nearest graphene layers, $a - d\cos\theta$, is along the x axis, which becomes clear by using the top view (b).

denote the NN hopping parameter within the graphene layer and η the hopping parameter between the nearest graphene layers. The intralayer NN bond length is denoted as a and the interlayer distance is equivalent to $d\sin\theta$. We define both η and γ to be positive without losing any generality.

If switching off the light, we can obtain the 2D standard graphene if we let $\eta = 0$, and a nonzero η destroys the C_3 symmetry but reserves inversion symmetry. Therefore, the band structure is gapless when η is less than γ. The gapless $\mathbf{k}$ points are nothing but special Dirac points defined with only two Pauli matrices, much like Dirac points in the 2D graphene. They can survive even when the light is turned on.

We use Floquet theory to study the time-dependent nonequilibrium systems [32,33], because the Hamiltonian (2) is periodic in time, $H(\mathbf{k},t) = H(\mathbf{k},t+T)$, where the time period is $T = 2\pi/w$. In terms of the Floquet-Bloch ansatz [34], the eigenstates can be written as $|\Psi_{\alpha,\mathbf{k}}(t)\rangle = e^{-i\varepsilon_{\alpha,\mathbf{k}}t}|u_{\alpha,\mathbf{k}}(t)\rangle$, where $\varepsilon_{\alpha,\mathbf{k}}$ stands for the quasienergy of the Floquet state, α is the band index, and $|u_{\alpha,\mathbf{k}}(t)\rangle$ is periodic in t. Substituting $|\Psi_{\alpha,\mathbf{k}}(t)\rangle$ into the Schrödinger equation leads to

$$[H(\mathbf{k},t) - i\partial_t]|u_{\alpha,\mathbf{k}}(t)\rangle = \varepsilon_{\alpha,\mathbf{k}}|u_{\alpha,\mathbf{k}}(t)\rangle. \tag{3}$$

We can define the Floquet Hamiltonian as

$$H_F = H(\mathbf{k},t) - i\partial_t. \tag{4}$$

Defining $|u_{\alpha,\mathbf{k},n}\rangle$ to be the Fourier transform of the periodic Floquet state $|u_{\alpha,\mathbf{k}}(t)\rangle$, and applying H_F on the basis $\{|u_{\alpha,\mathbf{k},n}\rangle\}$, we can explicitly express the operator H_F in terms of the composed Hilbert space $\mathcal{S} = \mathcal{H}\otimes\mathcal{T}$ [32], with inner product $\langle\langle\cdots\rangle\rangle = \int_0^T\langle\cdots\rangle dt/T$, where $\mathcal{T}$ is spanned by the T-periodic function. With the annihilation and creating operators $c_{\alpha,\mathbf{k}}(t)$ and $c^\dagger_{\alpha,\mathbf{k}}(t)$ Fourier expanded in $c_{\alpha,\mathbf{k},n}$ and $c^\dagger_{\alpha,\mathbf{k},n}$, H_F can be expressed in a block matrix form with its block elements [28]

$$\begin{aligned}(H_F)_{n,m} &= nw\delta_{n,m} + H_{m-n},\\ H_{m-n} &= \frac{1}{T}\int_0^T H(k,t)e^{iw(m-n)t}dt.\end{aligned} \tag{5}$$

Obviously, H_{m-n} are the Fourier modes of time periodic $H(\mathbf{k},t)$. Without much effort, one can write the Floquet Hamiltonian in the block matrix form

$$H_F(\mathbf{k}) = \begin{pmatrix} \ddots & \ddots & \ddots & \ddots & \ddots \\ \ddots & H_0 + w & H_1 & H_2 & \ddots \\ \ddots & H_{-1} & H_0 & H_1 & \ddots \\ \ddots & H_{-2} & H_{-1} & H_0 - w & \ddots \\ \ddots & \ddots & \ddots & \ddots & \ddots \end{pmatrix} \tag{6}$$

The 2×2 matrix block H_n can be expressed as

$$H_n = \frac{1}{T}\int_0^T dt\, H(\mathbf{k},t)e^{inwt} = \begin{pmatrix} 0 & (H_n)_{12} \\ (H_n)_{21} & 0 \end{pmatrix}. \tag{7}$$

Defining $v_i = e^{i\mathbf{k}\cdot\delta_i}$, we can write the matrix elements in Eq. (7) as

$$\begin{aligned}(H_n)_{12} &= \gamma\left\{J_{-n}(A_0a)v_1 + J_n\left(\frac{A_0a}{2}\right)(v_2+v_3)\right\}\\ &\quad + \eta e^{in\theta}J_{-n}(A_0d)e^{i\mathbf{k}\cdot\mathbf{d}},\\ (H_n)_{21} &= \gamma\left\{J_n(A_0a)v_1^* + J_{-n}\left(\frac{A_0a}{2}\right)(v_2^*+v_3^*)\right\}\\ &\quad + \eta e^{in\theta}J_n(A_0d)e^{-i\mathbf{k}\cdot\mathbf{d}},\end{aligned} \tag{8}$$

where J_n is the Bessel function of order n.

III. WEYL SEMIMETAL AND WEYL FERMIONS

A. Dirac and semi-Dirac points

Generally speaking, there are infinite Floquet energy subbands labeled with $m = 0,\pm1,\pm2,\ldots$. To begin with, we consider the high-frequency limit, where the frequency is much larger than the hopping parameters ($w \gg \gamma,\eta$). In this regime, the overlap between different Floquet subbands is negligible. As a result, the Floquet bands near the Fermi energy are determined by H_0, and the bands are gapless at points $\mathbf{k}^D_\pm = (0, \pm k_{y0}, 0)$ if the condition

$$\gamma\left[J_0(A_0a) + 2J_0\left(\tfrac{1}{2}A_0a\right)\cos\left(\tfrac{\sqrt{3}}{2}ak_{y0}\right)\right] + \eta J_0(A_0d) = 0 \tag{9}$$

is satisfied. These points, appearing in a pair, are similar to usual Dirac points in the case of graphene, and are presented as the crossing points circled with green in Fig. 2. Their low-energy effective Hamiltonian can be written as

$$\begin{aligned}H^{\mathrm{D}}_{\mathrm{eff}} &= h_1\sigma_1 + h_2\sigma_2,\\ h_1 &= -\sqrt{3}a\gamma J_0\left(\tfrac{1}{2}A_0a\right)\sin\left(\pm k_{y0}\tfrac{\sqrt{3}}{2}a\right)k_y,\\ h_2 &= a\gamma\left[J_0\left(\tfrac{1}{2}A_0a\right)\cos\left(k_{y0}\tfrac{\sqrt{3}}{2}a\right) - J_0(A_0a)\right]k_x\\ &\quad - \eta J_0(dA_0)\mathbf{k}\cdot\mathbf{d},\end{aligned} \tag{10}$$

where $\mathbf{k}$ is defined with respect to $\mathbf{k}^D_\pm$. We use usual definition for the Pauli matrices: $\sigma_1 = \sigma_x$, $\sigma_2 = \sigma_y$, and $\sigma_3 = \sigma_z$. These mean that in this frequency regime the system is a Dirac semimetal. When the light strength increases, the two gapless points will move toward the origin of the momentum space and will finally disappear at the origin, opening a semiconductor

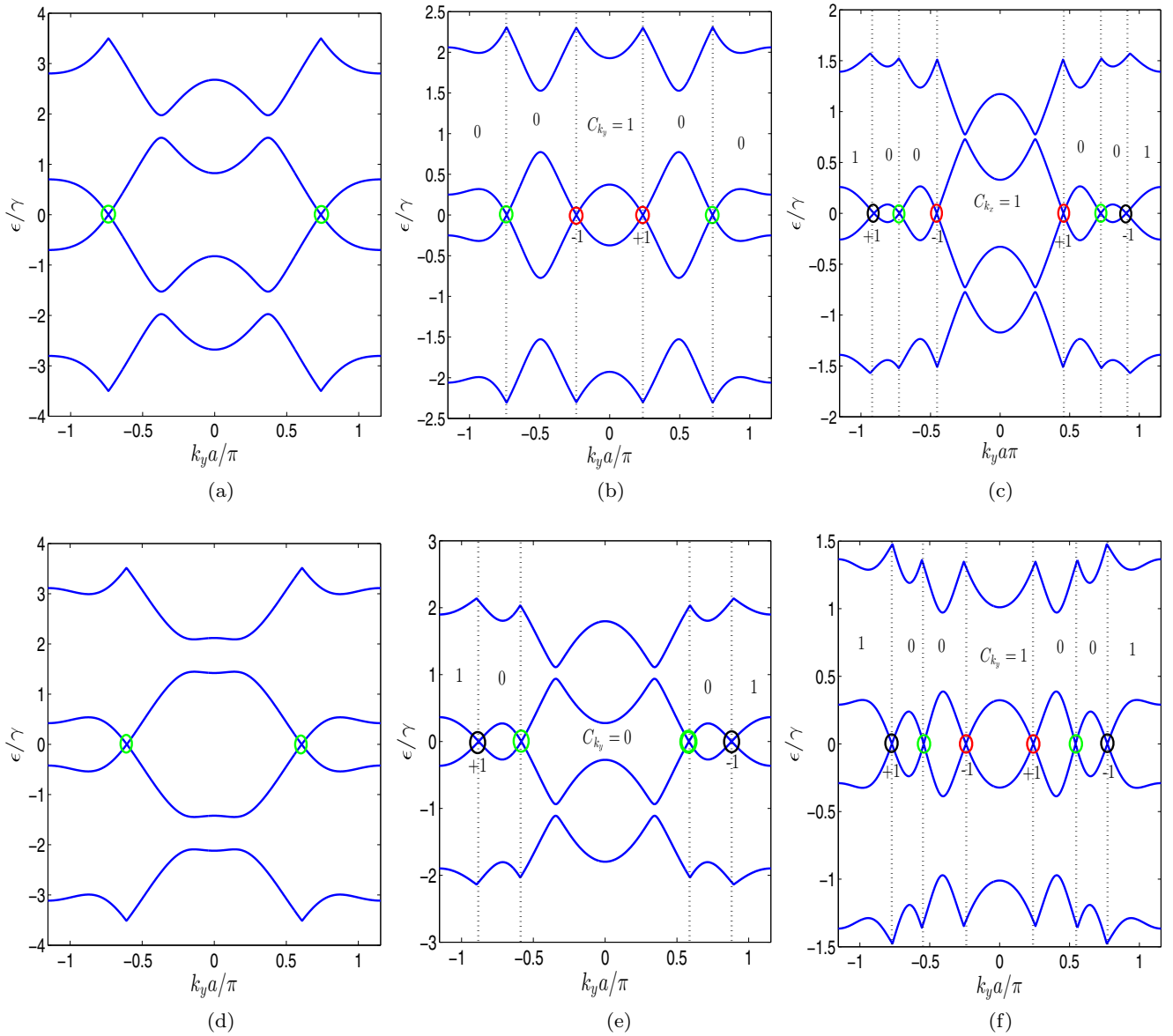

FIG. 2. The band structure along the k_y axis, with $k_x = k_z = 0$. For the A_0a values, there always exist two gapless Dirac points (denoted by green circles). For different frequencies, there can be one or two pairs of Weyl points astride $\mathbf{k}_0$ (red circles) and/or $\mathbf{k}_1$ (black circles). The H_F matrix is truncated at $m = \pm 2$, and other parameters are set as $d = 2a$, $\eta = \gamma/7$, and $\theta = 4\pi/9$. (a) $A_0a = 1$, $w = 3.5\gamma$ (b) $A_0a = 1$, $w = 2.3\gamma$ (c) $A_0a = 1$, $w = 1.5\gamma$ (d) $A_0a = 2$, $w = 3.5\gamma$ (e) $A_0a = 2$, $w = 2\gamma$ (f) $A_0a = 2$, $w = 1.3\gamma$.

gap and causing the Dirac semimetal to become an ordinary insulator.

When the frequency decreases further, there will be some overlapping between different Floquet subbands. While decreasing the frequency, at first the lower branch of the $m = 1$ subbands will intersect with the upper branch of the $m = 0$ subbands at $\varepsilon = w/2$, and meanwhile the upper branch of the $m = -1$ subbands will intersect with the lower branch of the $m = 0$ bands at $\varepsilon = -w/2$. As a rule, the near subbands whose m values differ by $\Delta m = \pm 1$ will intersect with each other. It should be pointed out that the perturbation introduced by $H_{\pm 1}$, that stands for the coupling of $m = \pm 1$ sub-bands and $m = 0$ subbands, can open energy gaps at the band crossing points. Here, we will concentrate on the band touching between the $m = \pm 1$ subbands at $\varepsilon = 0$. There is one touching point at $\mathbf{k}_0 = (0,0,0)$ when the condition

$$w = \gamma\left[J_0(A_0a) + 2J_0\left(\tfrac{1}{2}A_0a\right)\right] + \eta J_0(A_0d) \qquad (11)$$

is satisfied. Another touching point can appear at $\mathbf{k}_1 = (0, \frac{2}{\sqrt{3}a}\pi, 0)$ when the condition

$$w = \gamma\left[J_0(A_0a) - 2J_0\left(\tfrac{1}{2}A_0a\right)\right] + \eta J_0(A_0d) \qquad (12)$$

is satisfied. However, the w value can be modified by the perturbation of $H_{\pm 1}$ when the $m = \pm 1$ subbands toucheach other. Being different from the $\Delta m = \pm 1$ sub-bands touching, the perturbation of the $H_{\pm 2}$ block will be diagonal between the ± 1 subbands when we diagonalize the H_0 block along the k_y axis. That means the band touching points can be moved but cannot be removed by the perturbation. This trend can be seen in Fig. 2.

The $k \cdot p$ perturbation theory can be used to study the band structure near the two touching points at $\mathbf{k}_0 = (0,0,0)$ and $\mathbf{k}_1 = (0, \frac{2}{\sqrt{3}a}\pi, 0)$. It can be easily found that they are semi-Dirac points with an effective Hamiltonian

$$
\begin{aligned}
H_{\text{eff}}^{\text{SD}} &= \sum_{i=1}^{3} h_i(\mathbf{k})\sigma_i, \quad h_1(\mathbf{k}) = -2\eta \sin 2\theta J_2(A_0 d)\mathbf{k}\cdot\mathbf{d}, \\
h_2(\mathbf{k}) &= -2\gamma\left[J_2(A_0 a) \mp J_2\left(\tfrac{1}{2}A_0 a\right)\right]k_x a \\
&\quad - 2\eta \cos 2\theta J_2(A_0 d)\mathbf{k}\cdot\mathbf{d}, \\
h_3(\mathbf{k}) &= -\gamma\left\{J_0(A_0 a)(\mathbf{k}\cdot\mathbf{a}_1)^2 \pm J_0\left(\tfrac{1}{2}A_0 a\right)[(\mathbf{k}\cdot\mathbf{a}_2)^2\right. \\
&\quad \left. + (\mathbf{k}\cdot\mathbf{a}_3)^2]\right\} - \eta J_0(A_0 d)(\mathbf{k}\cdot\mathbf{d})^2, \qquad (13)
\end{aligned}
$$

where $\mathbf{k}$ is defined with respect to $\mathbf{k}_0$ or $\mathbf{k}_1$. The upper sign in both $\mp$ and $\pm$ in Eq. (13) is for $\mathbf{k}_0$, and the lower one for $\mathbf{k}_1$. These semi-Dirac points are similar to those in the 2D graphene formed by making the two Dirac points along the y axis meet when the C_3 symmetry was broken [35], but in that case, a gap is opened in the graphene's band structure after the two Dirac points are merged. Here, however, the two semi-Dirac points, independent of each other, cannot be merged, although they can coexist in some parameter regions.

B. Nontrivial Weyl points and Weyl fermions

The energy gap between the $m = \pm 1$ subbands is closed when the semi-Dirac point is created. When the frequency decreases further, the semi-Dirac point will split into two Weyl points at $\mathbf{k}_{\pm}^{W} = (0, \pm k_{yc}, 0)$, where k_{yc} is determined by the equation

$$
w = \gamma\left[J_0(A_0 a) + 2J_0\left(\tfrac{1}{2}A_0 a\right)\cos\left(\tfrac{\sqrt{3}}{2}a k_{yc}\right)\right] + \eta J_0(A_0 d). \qquad (14)
$$

Similarly the effective Hamiltonian can be obtained by the $k \cdot p$ perturbation theory, reading

$$
\begin{aligned}
H_{\text{eff}}^{\text{W}} &= \sum_{i,j=1}^{3} v_{ij} k_i \sigma_j, \quad v_{11} = -2\eta \sin 2\theta J_2(A_0 d) d \cos\theta, \\
v_{12} &= 2a\gamma\left[J_2\left(\tfrac{1}{2}A_0 a\right)\cos\left(k_{yc}\tfrac{\sqrt{3}}{2}a\right)\right. \\
&\quad \left. - J_2(A_0 a)\right] - 2\eta\cos 2\theta J_2(A_0 d) d\cos\theta, \\
v_{23} &= 2\sqrt{3}a\gamma J_2\left(\tfrac{1}{2}A_0 a\right)\sin\left(\pm k_{yc}\tfrac{\sqrt{3}}{2}a\right), \qquad (15) \\
v_{31} &= 2\eta \sin 2\theta J_2(A_0 d) d \sin\theta, \\
v_{32} &= 2\eta \cos 2\theta J_2(A_0 d) d \sin\theta, \\
v_{13} &= v_{21} = v_{22} = v_{33} = 0,
\end{aligned}
$$

where $\mathbf{k}$ is defined with respect to $\mathbf{k}_{\pm}^{W}$. It is interesting that the low-energy Hamiltonians for the Weyl point pairs astride both $\mathbf{k}_0$ and $\mathbf{k}_1$ have the same form. If we let k_{yc} be equal to either 0 or $\frac{2}{\sqrt{3}a}\pi$, the v_{23} term will disappear and the quadric term will return, resuming a semi-Dirac point again.

We can calculate the Weyl number using the definition

$$
\begin{aligned}
C &= \text{sgn}[\det[v]] \\
&= \text{sgn}\left\{4\sqrt{3}a^2\gamma J_2\left(\tfrac{1}{2}A_0 a\right)\sin\left(k_{yc}\tfrac{\sqrt{3}}{2}a\right)\right. \\
&\quad \left.\times\left[J_2\left(\tfrac{1}{2}A_0 a\right)\cos\left(k_{yc}\tfrac{\sqrt{3}}{2}a\right) - J_2(A_0 a)\right]\right\} \qquad (16)
\end{aligned}
$$

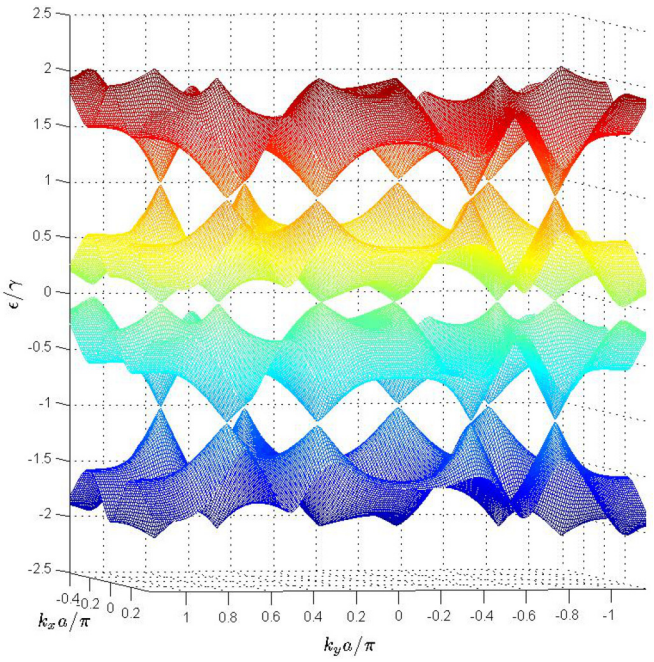

FIG. 3. The band structures of the $m = 0$ and $m = \pm 1$ subbands in the $k_z = 0$ plane, with parameters $\eta = \gamma/7$, $A_0 a = 1.5$, $w = 2\gamma$, $d = 2a$, and $\theta = 4\pi/9$. Two pairs of Weyl points are symmetrical astride $\mathbf{k}_0$ and $\mathbf{k}_1$, respectively.

It can be proved that the two Weyl points possess opposite Weyl number or chirality. The Weyl points created by the band crossing of the $m = \pm 1$ subbands, with their Weyl numbers labeled, are shown in Fig. 3.

C. Phase diagram

When the frequency decreases, the distance between the two Weyl points in a pair increases, and k_{yc} can approach k_{y0} but cannot exceed it. Thus, in this frequency regime, the system will stay in a WSM phase, with one pair of Weyl points or two if one or both of the semi-Dirac points (corresponding to $\mathbf{k}_0$ and $\mathbf{k}_1$) were created and then split. On the other hand, for the very strong light amplitude, we should have an ordinary insulator phase in the regime of high frequency. In this strong light regime ($A_0 a \geqslant 4.13$), there can be a pair of Weyl points astride $\mathbf{k}_1$ when the frequency becomes enough low. The complete phase diagram is presented in Fig. 4. Here, $\theta = 4\pi/9$ is used. The ABC stacking is obtained if we set $\theta = \pi/2$, but we need $\theta \neq \pi/2$ to achieve nontrivial topological properties. We have six phases in the phase diagram: semimetal (SM), Weyl semimetal with one pair of Weyl fermions astride $\mathbf{k}_0$ (WSM1-A), Weyl semimetal with one pair of Weyl fermions astride $\mathbf{k}_1$ (WSM1-B), Weyl semimetal with two pairs of Weyl fermions (WSM2), ordinary insulator (I), and Weyl semimetal (WSM). There are Dirac points in the former four phases, but there exist no Dirac points in the I and WSM phases.

It can be seen that for $0 \leqslant A_0 a < 1.34$ and $1.34 < A_0 a \leqslant 4.13$, there are two phase transitions with the frequency decreasing: (1) from SM to WSM1-A/WSM1-B and (2) from WSM1-A/WSM1-B to WSM2. At the special point $A_0 a = 1.34$, the two phase transitions are replaced by one:

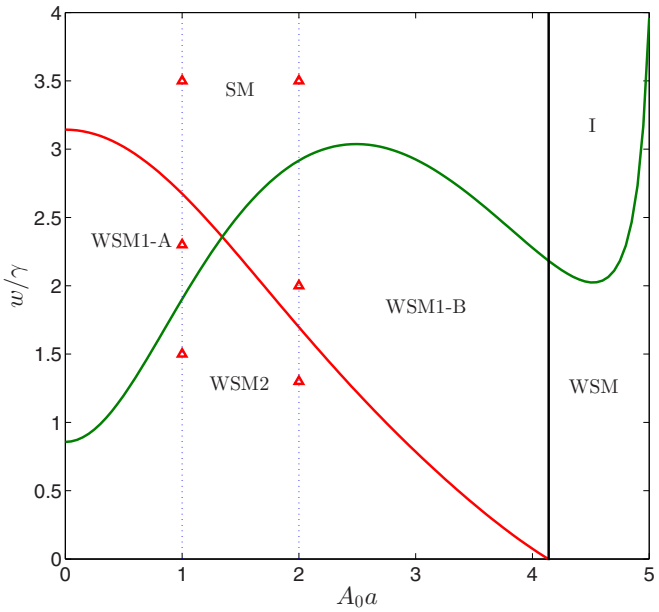

FIG. 4. The phase diagram with experimentally achievable [31] parameters $d = 2a$, $\eta = \gamma/7$, and $\theta = 4\pi/9$. There are six phases: semimetal (SM), Weyl semimetal with one pair of Weyl fermions astride $\mathbf{k}_0$ (WSM1-A), Weyl semimetal with one pair of Weyl fermions astride $\mathbf{k}_1$ (WSM1-B), Weyl semimetal with two pairs of Weyl fermions (WSM2), ordinary insulator (I), and Weyl semimetal (WSM). The six triangles show the $(\omega/\gamma, A_0a)$ values for the band structures shown in Fig. 2.

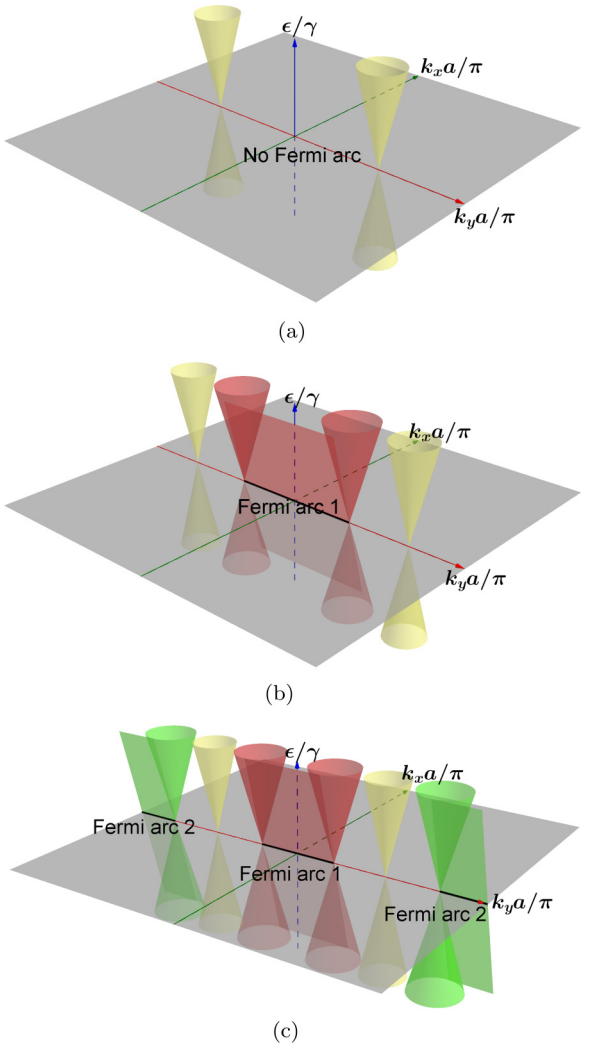

FIG. 5. The frequency dependence of the Fermi arcs in the surface Brillouin zone: (a) no Fermi arc for $w \sim 3.5\gamma$ in the SM phase, (b) one Fermi arc near $(k_x,k_y) = (0,0)$ for $w \sim 2.3\gamma$ in the WSM1-A phase, and (c) two Fermi arcs near $(k_x,k_y) = (0,0)$ and $(0,\pi/a)$ for $w \sim 1.5\gamma$ in the WSM2 phase. Here the light amplitude is $A_0a < 1$. (a) No Fermi arc in the SM phase.(b) One Fermi arc in the WSM1-A phase.(c) Two Fermi arcs in the WSM2 phase.

from SM to WSM2. It is clear that there are WSM phases even in the low-amplitude limit $A_0a \to 0$. This feature of the phase diagram is different from that in Ref. [25], where a WSM phase is obtained from a quantum anomalous Hall phase when the light amplitude exceeds a threshold value. The threshold should be due to two-order virtual photon processes considered in high frequency regime. In contrast, our cases are beyond the high frequency regime and we treat H_0 and $H_{\pm1}$ accurately. It should be pointed out that when the light frequency enters deeply the WSM2 phase, other subbands need to be considered and more pairs of Weyl points will appear. This situation is similar to hierarchy of Floquet gaps in two-dimensional driven honeycomb lattices [36].

D. Surface states and finite multilayers

One of the most striking phenomena in a WSM phase is its Fermi arc in the surface Brillouin zone. We can address it in a simple way [5,12]. In our case, $H_{\rm eff}^{\rm W}(k_x,k_y,k_z)$ with a given k_y can be considered such a 2D (k_x,k_z) Hamiltonian and one can calculate its k_y-dependent Chern number C_{k_y}. It is well known that for a 2D Hamiltonian one can change its Chern number by changing its parameters [12]. In our case, the Chern number will change by

$$\Delta C = C_{k_y} - C_{k_y'} \tag{17}$$

when k_y crosses a Weyl point where the mass term changes sign. It is easy to get $C_{k_y} = 1$ when k_y is between the two Weyl points in each pair, and $C_{k_y} = 0$ otherwise. Semi-Dirac points do not change the Chern number because the $H_{\rm eff}^{\rm SD}$ near it has no mass term. We already illustrated the Chern numbers in Fig. 2. Because k_y is kept as a good quantum number, each nontrivial 2D Hamiltonian, with $C_{k_y} = 1$ and gapped bulk states, has zero-mode edge states along its 1D boundary. The edge states will disappear into the bulk states at the Weyl points and thus the locus of the edge states makes the Fermi arc which connects the projections of each pair of Weyl points in the surface Brillouin zone. Therefore, as long as the flat surface is parallel to the k_y axis, a Fermi arc will emerge in the surface Brillouin zone.

We can create a natural surface at $z = 0$ by cleaving the the infinite graphene layers, which keeps k_x and k_y as good quantum numbers. This is similar to the surface created for layered NbP [37]. We demonstrate in Fig. 5 the development of the Fermi arcs by decreasing the frequency, where the surface is perpendicular to the k_z axis and the light amplitude parameter

is set to $A_0 a < 1$. There is no Fermi arc in Fig. 5(a) because there are no Weyl fermions for $w \sim 3.5\gamma$ in the SM phase. One Fermi arc appears near $(k_x,k_y) = (0,0)$ in Figs. 5(b) and 5(c) because the two frequency values are in the WSM1-A phase and the WSM2 phase, respectively. In addition, there is a Fermi arc near $(k_x,k_y) = (0,\pi/a)$ in Fig. 5(c) because there are two pairs of Weyl fermions in the WSM2 phase. There exists a correspondence between the Weyl fermion pair and the Fermi arc.

It is clear that to experimentally realize the Floquet Weyl fermions, some appropriate multilayer structures are better than the infinitely stacked graphene model. On the basis of the above surface construction, we can construct finite stacked graphene models under circularly polarized light. Such finitely stacked models irradiated by circularly polarized light can be realized experimentally because the parameter θ can be made different from $\pi/2$ (90°) by bending the finite ABC-stacked graphene layers within the x-z plane [31]. For such models with the number of graphene layers being large enough, there are two natural surfaces perpendicular to the z axis, and k_x and k_y are good quantum numbers. As a result, there will be zero-mode edge states between the projections of each pair of the Weyl points in the two surface Brillouin zones. Therefore, they can host bulk Floquet Weyl fermions and surface Fermi arcs. Angle-resolved photoemission spectroscopy (ARPES) can be used to investigate these bulk Floquet Weyl fermions and surface Fermi arcs, because these systems are similar to 3D layered Weyl semimetal materials: NbP, TaP, and TaAs [20,22,37].

IV. FURTHER DISCUSSION AND CONCLUSION

To experimentally realize Floquet Weyl fermions in such graphene-based models, one has to prepare a circularly polarized light of suitable frequency and amplitude. Because the NN hopping constants ($\gamma \approx 2.8$ eV, $a \approx 1.4$ Å) are very large, we seem to need a high frequency (order of magnitude of $\sim 10^{16}$ Hz) and a strong amplitude (order of magnitude of $\sim 10^{8}$ V/m). However, as shown in the phase diagram in Fig. 4, the Floquet Weyl fermions can be realized when the frequency is low or the amplitude is weak. Nevertheless, it should be pointed out that in the regime of low frequency, other Floquet subbands, such as those with $\Delta m = 4,6,8$, will play roles in creating Floquet Weyl points at $\epsilon = 0$, and therefore some complex situations may appear. This is similar to some hierarchy structures in driven two-dimensional honeycomb lattices [36]. Fortunately, in the regime of weak light amplitude, one can realize the Weyl fermions in the region of $A_0 a < 0.5$ and $w < \gamma$ in the phase diagram. That is to say, 10^{15} Hz (ultraviolet), or even smaller than 10^{14} Hz (infrared), is large enough to achieve such Weyl fermions. Therefore, one can realize one or two pairs of Floquet Weyl fermions at experimentally achievable frequency levels [30,38].

In addition, some self-assembled graphene-like lattices of CdSe nanostructures [28,39,40] can be used to realize such Floquet Weyl fermions. Because their hopping parameters are approximately two order of magnitude smaller compared to graphene and their lattice constant is one order of magnitude larger, much lower frequency (10^{13} Hz or lower) is enough to realize Floquet Weyl fermions in good multilayer structures of such CdSe nanostructures [31].

In conclusion, we have proposed an interesting method to create Floquet Weyl fermions with a two-component semi-Dirac parent in a 3D stacked graphene system irradiated by circularly polarized light instead of a four-component Dirac parent. One or two semi-Dirac points can appear at $\mathbf{k_0} = (0,0,0)$ and/or $\mathbf{k_1} = (0, \frac{2}{\sqrt{3}a}\pi, 0)$ in momentum space when the frequency w of light is on the order of magnitude of hopping parameters γ and η. Upon decreasing the light frequency, each semi-Dirac point will split into two symmetrical Weyl points with opposite chirality. Further decreasing the frequency will make the Weyl points move in the momentum space, and the Weyl points can approach the Dirac points when the frequency becomes very small. The frequency-amplitude phase diagram has been worked out. It is clear that the Floquet Weyl femions, always appearing in pairs, can be created in the limit of low light amplitude, not needing any finite threshold for light amplitude [25]. This is because we treat H_0 and $H_{\pm 1}$ accurately, without requiring usual high-frequency limit [25]. Furthermore, it has been shown that there exist Fermi arcs in the surface Brillouin zones in semi-infinitely stacked and finitely multilayered graphene systems irradiated by circularly polarized light. These theoretical results can lead to a new platform to create Weyl fermions in graphene-based and similar systems.

ACKNOWLEDGMENTS

This work is supported by the National Natural Science Foundation of China (Grants No. 11174359 and No. 11574366), by the Chinese Department of Science and Technology (Grant No. 2012CB932302), and by the Strategic Priority Research Program of the Chinese Academy of Sciences (Grant No. XDB07000000).

[1] H. Weyl, Electron and gravitation, Z. Phys. **56**, 330 (1929).
[2] H. B. Nielsen and M. Ninomiya, The Adler-Bell-Jackiw anomaly and Weyl fermions in a crystal, Phys. Lett. B **130**, 389 (1983).
[3] S. Murakami, Phase transition between the quantum spin Hall and insulator phases in 3D: Emergence of a topological gapless phase, New J. Phys. **9**, 356 (2007).
[4] A. A. Burkov and L. Balents, Weyl Semimetal in a Topological Insulator Multilayer, Phys. Rev. Lett. **107**, 127205 (2011).
[5] X. Wan, A. M. Turner, A. Vishwanath, and S. Y. Savrasov, Topological semimetal and Fermi-arc surface states in the electronic structure of pyrochlore iridates, Phys. Rev. B **83**, 205101 (2011).
[6] L. Balents, Viewpoint: Weyl electrons kiss, Physics **4**, 36 (2011).
[7] G. Xu, H. Weng, Z. Wang, X. Dai, and Z. Fang, Chern Semimetal and the Quantized Anomalous Hall Effect in $HgCr_2Se_4$, Phys. Rev. Lett. **107**, 186806 (2011).
[8] K.-Y. Yang, Y.-M. Lu, and Y. Ran, Quantum Hall effects in a Weyl semimetal: Possible application in pyrochlore iridates, Phys. Rev. B **84**, 075129 (2011).
[9] Z. Wang, Y. Sun, X.-Q. Chen, C. Franchini, G. Xu, H. Weng, X. Dai, and Z. Fang, Dirac semimetal and topological phase

transitions in A_3Bi (A = Na, K, Rb), Phys. Rev. B **85**, 195320 (2012).

[10] D. T. Son and B. Z. Spivak, Chiral anomaly and classical negative magnetoresistance of Weyl metals, Phys. Rev. B **88**, 104412 (2013).

[11] Z. Wang, H. Weng, Q. Wu, X. Dai, and Z. Fang, Three-dimensional Dirac semimetal and quantum transport in Cd_3As_2, Phys. Rev. B **88**, 125427 (2013).

[12] O. Vafek and A. Vishwanath, Dirac fermions in solids: From high T_c cuprates and graphene to topological insulators and Weyl semimetals, Annu. Rev. Condens. Matter. Phys. **5**, 83 (2014).

[13] Z. K. Liu, B. Zhou, Y. Zhang, Z. J. Wang, H. M. Weng, D. Prabhakaran, S.-K. Mo, Z. X. Shen, Z. Fang, X. Dai, Z. Hussain, and Y. L. Chen, Discovery of a three-dimensional topological Dirac semimetal Na_3Bi, Science **343**, 864 (2014).

[14] Z. K. Liu, J. Jiang, B. Zhou, Z. J. Wang, Y. Zhang, H. M. Weng, D. Prabhakaran, S. K. Mo, H. Peng, P. Dudin, T. Kim, M. Hoesch, Z. Fang, X. Dai, Z. X. Shen, D. L. Feng, Z. Hussain, and Y. L. Chen, A stable three-dimensional topological Dirac semimetal Cd_3As_2, Nat. Mater. **13**, 677 (2014).

[15] S. Borisenko, Q. Gibson, D. Evtushinsky, V. Zabolotnyy, B. Büchner, and R. J. Cava, Experimental Realization of a Three-Dimensional Dirac Semimetal, Phys. Rev. Lett. **113**, 027603 (2014).

[16] M. Neupane, S.-Y. Xu, R. Sankar, N. Alidoust, G. Bian, C. Liu, I. Belopolski, T.-R. Chang, H.-T. Jeng, H. Lin, A. Bansil, F. Chou, and M. Z. Hasan, Observation of a three-dimensional topological Dirac semimetal phase in high-mobility Cd_3As_2, Nat. Commun. **5**, 3786 (2014).

[17] S.-Y. Xu, C. Liu, S. K. Kushwaha, R. Sankar, J. W. Krizan, I. Belopolski, M. Neupane, G. Bian, N. Alidoust, T.-R. Chang, H.-T. Jeng, C.-Y. Huang, W.-F. Tsai, H. Lin, P. P. Shibayev, F.-C. Chou, R. J. Cava, and M. Z. Hasan, Observation of Fermi arc surface states in a topological metal, Science **347**, 294 (2015).

[18] H. Weng, C. Fang, Z. Fang, B. A. Bernevig, and X. Dai, Weyl Semimetal Phase in Noncentrosymmetric Transition-Metal Monophosphides, Phys. Rev. X **5**, 011029 (2015).

[19] S.-M. Huang, S.-Y. Xu, I. Belopolski, C.-C. Lee, G. Chang, B. Wang, N. Alidoust, G. Bian, M. Neupane, C. Zhang, S. Jia, A. Bansil, H. Lin, and M. Z. Hasan, A Weyl Fermion semimetal with surface Fermi arcs in the transition metal monopnictide TaAs class, Nat. Commun. **6**, 7373 (2015).

[20] S.-Y. Xu, I. Belopolski, N. Alidoust, M. Neupane, G. Bian, C.-L. Zhang, R. Sankar, G.-Q Chang, Z. Yuan, C.-C. Lee, S.-M. Huang, H. Zheng, J. Ma, D. S. Sanchez, B. Wang, A. Bansil, F. Chou, P. P. Shibayev, H. Lin, S. Jia, and M. Z. Hasan, Discovery of a Weyl fermion semimetal and topological Fermi arcs, Science **349**, 613 (2015).

[21] L. Lu, Z. Wang, D. Ye, L. Ran, L. Fu, J. D. Joannopoulos, and M. Soljačić, Experimental observation of Weyl points, Science **349**, 622 (2015).

[22] B. Q. Lv, H. M. Weng, B. B. Fu, X. P. Wang, H. Miao, J. Ma, P. Richard, X. C. Huang, L. X. Zhao, G. F. Chen, Z. Fang, X. Dai, T. Qian, and H. Ding, Experimental Discovery of Weyl Semimetal TaAs, Phys. Rev. X **5**, 031013 (2015).

[23] K. Fukushima, D. E. Kharzeev, and H. J. Warringa, Chiral magnetic effect, Phys. Rev. D **78**, 074033 (2008).

[24] P. B. Pal, Dirac, Majorana, and Weyl fermions, Am. J. Phys. **79**, 485 (2011).

[25] R. Wang, B. Wang, R. Shen, L. Sheng, and D. Y. Xing, Floquet Weyl semimetal induced by off-resonant light, Europhys. Lett. **105**, 17004 (2014).

[26] A. Gómez-León and G. Platero, Floquet-Bloch theory and topology in periodically driven lattices, Phys. Rev. Lett. **110**, 200403 (2013).

[27] A. Kundu, H. A. Fertig, and B. Seradjeh, Effective Theory of Floquet Topological Transitions, Phys. Rev. Lett. **113**, 236803 (2014).

[28] A. Quelle, M. Goerbig, and C. M. Smith, Artificial graphene under the spotlight: A realisation of the Bernevig-Hughes-Zhang model, New J. Phys. **18**, 015006 (2016).

[29] N. H. Lindner, G. Refael, and V. Galitski, Floquet topological insulator in semiconductor quantum wells, Nat. Phys. **7**, 490 (2011).

[30] M. A. Sentef, M. Claassen, A. F. Kemper, B. Moritz, T. Oka, J. K. Freericks, and T. P. Devereaux, Theory of Floquet band formation and local pseudospin textures in pump-probe photoemission of graphene, Nat. Commun. **6**, 7047 (2015).

[31] T. Korhonen and P. Koskinen, Peeling of multilayer graphene creates complex interlayer sliding patterns, Phys. Rev. B **92**, 115427 (2015).

[32] H. Sambe, Steady states and quasienergies of a quantum-mechanical system in an oscillating field, Phys. Rev. A **7**, 2203 (1973).

[33] A. Hemmerich, Effective time-independent description of optical lattices with periodic driving, Phys. Rev. A **81**, 063626 (2010).

[34] G. Platero and R. Aguado, Photon-assisted transport in semiconductor nanostructures, Phys. Rep. **395**, 1 (2004).

[35] B. A. Bernevig and T. L. Hughes, *Topological Insulators and Topological Superconductors* (Princeton University Press, Princeton, 2013).

[36] P. M. Perez-Piskunow, L. E. F. F. Torres, and G. Usaj, Hierarchy of Floquet gaps and edge states for driven honeycomb lattices, Phys. Rev. A **91**, 043625 (2015).

[37] Z. K. Liu, L. X. Yang, Y. Sun, T. Zhang, H. Peng, H. F. Yang, C. Chen, Y. Zhang, Y. F. Guo, D. Prabhakaran, M. Schmidt, Z. Hussain, S.-K. Mo, C. Felser, B. Yan, and Y. L. Chen, Evolution of the Fermi surface of Weyl semimetals in the transition metal pnictide family, Nat. Mater. **15**, 27 (2016).

[38] P. B. Corkum and F. Krausz, Attosecond science, Nat. Phys. **3**, 381 (2007).

[39] E. Kalesaki, C. Delerue, C. M. Smith, W. Beugeling, G. Allan, and D. Vanmaekelbergh, Dirac Cones, Topological Edge States, and Nontrivial Flat Bands in Two-Dimensional Semiconductors with a Honeycomb Nanogeometry, Phys. Rev. X **4**, 011010 (2014).

[40] M. P. Boneschanscher, W. H. Evers, J. J. Geuchies, T. Altantzis, B. Goris, F. T. Rabouw, S. van Rossum, H. S. J. van der Zant, L. D. A. Siebbeles, G. van Tendeloo, I. Swart, J. Hilhorst, A. V. Petukhov, S. Bals, and D. Vanmaekelbergh, Long-range orientation and atomic attachment of nanocrystals in 2D honeycomb superlattices, Science **344**, 1377 (2014).